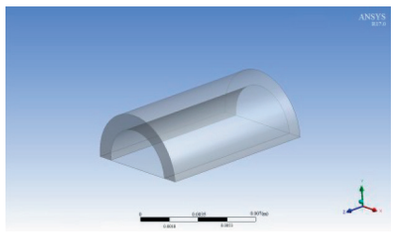
Mechanical properties of 3D-printed blood vessels



Propiedades mecánicas de vasos sanguíneos impresos en 3D

Jiyan Wang[1*], Srikumar Krishnamoorthy[2], Hongtao Song[3], Changhong Ma[1]

[1] School of Science, Shandong Jiaotong University, Jinan, Shandong Province, 250357, China; * Corresponding author, Email: wangjiyan2004@126.com
[2] Department of Industrial and Systems Engineering, Texas Tech University, Lubbock, TX 79409, USA
[3] Department of Mechanical Engineering, the University of Texas at Austin, Austin, TX 78712, USA

DOI: http://dx.doi.org/10.6036/9719 | Recibido: 04/03/2020 • Inicio Evaluación: 04/03/2020 • Aceptado: 21/04/2020

RESUMEN

- La demanda de sustitutos vasculares en la práctica clínica ha aumentado, y los vasos sanguíneos impresos en 3D podrían ser alternativas ventajosas. Determinar las propiedades mecánicas de los vasos sanguíneos impresos en 3D es importante para mejorar aún más la tecnología y la aplicación clínica. En este caso, se prepararon probetas "dogbone" con y sin células mediante la impresión en 3D con un curado combinado de luz ultra violeta (UV) y de iones químicos en el hidrogel. Se realizaron pruebas de tracción para medir los parámetros mecánicos de las probetas "dogbone" y construir dos tipos de modelos de interacción fluido-sólido. De acuerdo con los teoremas de hidrodinámica y de la cantidad de movimiento, se seleccionaron como velocidades de entrada las velocidades en el período de eyección acelerado, el pico de eyección, el período de eyección reducido y el período diastólico temprano. Se analizó la distribución de la velocidad en la superficie de simetría del fluido y el estrés y la tensión del tubo sólido bajo diferentes velocidades. Los resultados revelan que la velocidad disminuye gradualmente desde el centro del fluido hasta la pared. A una alta velocidad de entrada, la velocidad del fluido es alta, mientras que la tensión y el esfuerzo de la pared aumentan. Durante el pico de eyección cardíaca, la tensión en la pared alcanza el valor máximo de 2018 Pa, que es mucho menor que la tensión final. Además, la resistencia y la rigidez disminuyen para los vasos que contienen células. Este trabajo proporciona un método factible para medir las propiedades mecánicas de los vasos sanguíneos impresos en 3D.
- **Palabras clave:** Impresión 3D, propiedades mecánicas, interacción fluido-sólido.

ABSTRACT

The demand for vascular substitutes in clinical practice has increased, and 3D-printed blood vessels could be advantageous alternatives. Determining the mechanical properties of 3D-printed blood vessels is important to further improve the technology and clinical application. Here, dogbones with and without cells were generated by 3D printing with combined UV curing and hydrogel ion curing. Tensile tests were performed to measure the mechanical parameters of the dogbones and build two kinds of fluid–solid interaction models. In accordance with hydrodynamics and momentum theorems, the velocities in accelerated ejection period, ejection peak, reduced ejection period, and early diastolic period were selected as inlet velocities. Velocity distribution on the symmetry surface of the fluid and the stress and strain of the solid tube under different velocities were analyzed. Results reveal that the velocity decreases gradually from the fluid center to the wall. At a high inlet velocity, the fluid velocity is high, while the stress and strain of the wall increase. During cardiac ejection peak, the stress on the wall reaches the maximum value of 2018 Pa, which is much lower than the ultimate stress. In addition, the strength and stiffness decrease for the vessels added with cells. This work provides a feasible method for measuring the mechanical properties of 3D-printed blood vessels.

Keywords: 3D printing, mechanical properties, fluid–solid interaction.

1. INTRODUCTION

Cardio-cerebrovascular diseases are the leading cause of death. The clinical demand for blood vessels has increased with the number of such diseases.[1,2] At present, the common primary and auxiliary treatment for severe patients is vascular transplantation; however, autologous blood vessels are limited. Therefore, a large number of artificial blood vessels are needed for transplantation. Among the different kinds of manufacturing methods for artificial blood vessels, 3D bio-printing has many advantages. Some of the methods for this rapid prototyping or additive manufacturing technology include inkjet printing, extrusion printing, and stereolithography, which can produce multi-scale, multi-material, and multi-cellular tissues with heterogeneity and functional intrinsic structure. Bioactive vascular prostheses are used in clinical trials for congenital heart disease,[3] peripheral artery disease,[4] and hemodialysis vascular reconstruction.[5,6]

Owing to the differences in mechanical and biological properties and rapid gel mechanism between natural and printed blood vessels with complex printing conditions, the 3D printing of composite vessels with good biocompatibility is still at the primary stage. Studying the mechanical properties of 3D-printed vascular materials and the interaction between natural and 3D-printed blood vessels is important in selecting the appropriate 3D vascular printing materials and improving the methods.

Scholars worldwide have extensively studied 3D blood vessel printing[7-12]. However, the characteristics of 3D-printed vascular materials and the coupling relationship between natural and 3D-printed blood vessels are still poorly understood. Developing a rapid printing method for blood vessels and clarifying the coupling relationship between natural and 3D-printed blood vessels are necessary.

This study adopts the 3D printing method of combining UV curing and ion curing to print two kinds of dogbone to precisely predict the properties of 3D-printed blood vessels and provide references for their clinical application. Two fluid–solid interaction models were also built, and the mechanical characteristics of the fluid and solid were analyzed.

2. STATE OF THE ART

Researchers have extensively studied the materials, methods, processes, and functions of 3D blood vessel printing. Hydrogels have been used as a printing material to print solid tube. Hydrogel, which is soft in nature, can maintain a certain shape, absorb a large amount of water, wrap cells, support printing structure, and thus is often used in 3D bio-printing. The commonly employed bio-hydrogel includes sodium alginate, gelatin, hyaluronic acid, poly (ethylene glycol) diacrylate (PEGDA), and gelatine methacrylate (GelMA). Yu et al. [13] printed hollow sodium alginate tubes by coaxial nozzle on the basis of the gelling principle of sodium alginate and calcium chloride solutions and analyzed the influences of various technological parameters on the size of hollow tubes and the transportation of cell culture fluid. However, the mechanical strength of printed hollow tube cannot meet the application requirements. Mao et al. [14] built a coaxial nozzle printing system. After the addition of 0.25% ferric chloride solution, the mechanical strength and biocompatibility of the tube were enhanced. Freeman et al. [15] incorporated fibrinogen with gelatin to produce bio-ink, used biological printer to print blood vessels, analyzed the effects of gelatin concentration and heat treatment on viscosity and mechanical performance of 3D-printed blood vessels, and emphasized that the bio-ink formula is important for the performance of printed blood vessels. Many scholars attempted to improve printing efficiency and accuracy by focusing on methods and processes. Wu et al. [16-20] studied the 3D printing of blood vessels by adjusting multiple parameters. Yu et al. [21] used the ink-jet method to print the circular tube and proposed the use of non-circular printing path to offset the deformation caused by gravity and impact force of the tube to improve printing accuracy. The successful application of 3D cell printing provided new ideas for the 3D printing of blood vessels. Xu et al. [22-27] prepared bio-ink containing cells and successfully printed biological vessels through various methods. Ho et al. [28-30] prepared the 3D printing model of the aorta, successfully copied the aortic structure, and applied 3D printing for preoperative planning. Wang et al. [31] conducted simulation studies on the relationship between 3D-printed artificial blood vessel wall and internal liquid flow field. The effects of different wall topology, structure size, and viscosity on the internal flow field of artificial vessels were studied by using the Comsol software.

The above studies mainly focused on improving the printing accuracy and mechanical strength of the printing model; however, works on the mechanical properties, especially on the dynamic characteristics of the 3D printing model with cells, are limited. In the present study, dogbones with and without cells were 3D printed through combined UV curing and ion curing. A fluid–solid interaction model was built based on the mechanical property tests. Under different inlet velocities, the dynamic characteristics of the fluid, the force and deformation of the solid tubes, and the relationship between flow velocity and the mechanical properties of the printing material were discussed to support the findings.

The remainder of this study is organized as follows. Section 3 describes the process of 3D printing, the relevant parameters of printing materials, and the construction of the model of fluid and vascular coupling. Section 4 provides the analysis of the relationship between fluid and solid through finite element method and discusses the characteristics of fluid and solid under different velocities. Section 5 summarizes the conclusions.

3. MECHANICAL PROPERTIES AND CELL VIABLILITY

3.1. HYDROGEL FORMULATION

Exactly 300 mg of sodium alginate, 30 ml of phosphate buffer saline (PBS), 300 mg of GelMA, and 15 mg of irgacure 2959 were mixed in the solution. Alginate and GelMA are polymeric materials, and PBS is generally employed as a solvent to dissolve protective reagents and can also serve as buffer and provide bivalent cations. As a photo-initiator, Irgacure 2959 absorbs light energy and is divided into two active free radicals when irradiated by ultraviolet light, leading to the chain polymerization of photosensitive resin and active diluent and crosslinking with the adhesive. The mixture was stirred fully, placed in the incubator, and allowed to stand for 4 h until the solution became clear. This mixture is the hydrogel formulation without cells. The same solution was prepared again and mixed with 30×10^6 NIH 3T3 fibrobalsts. The hydrogel with cells was obtained when the cell concentration reached 1×10^6 cells/ml.

3.2. 3D PRINTING



(a) Dogbone without cells



(b) Dogbone with cells

Fig. 1 Sample before tensile test

The devices for 3D printing include digital micro-mirror device (DMD, Wintech W4100 develop kit) and UV (Omnicure S2000) printing models. The light projected by DMD contains UV light. In the projected area, UV light was fully combined with UV photosensitive resin Irgacure 2959. The printed materials were cured and molded. The UV exposure time is approximately 40 s, and the light intensity is 6.9 mW/cm^2. Finally, the dogbones with and without cells were printed.

The dogbones were submerged in 2% (w/v) $CaCl_2$ solution for 15 min. Ca^{2+} was then fully cross-linked with the alginate, resulting in further ionic curing. The short submerging period had minimal influence on the weight or shape of these dogbones. After the calculation, the swelling ratio (additional weight after submerging over original weight) is only approximately 5%. The cured models shown in Fig. 1 were obtained. Fig. 1(a) shows the dogbone without cells, and Fig. 1(b) the dogbone with cells.

3.3. MECHANICAL PROPERTIES

Tensile tests were performed for two kinds of printed dogbones (ASTM D412). Three pieces of each sample were measured, and the dimensions of the samples are shown in Table I. The dogbone samples with and without cells were placed on the DMA Q800

test machine as shown in Fig. 2. The drawing speed was set to 10%/min and strain control in 70%. The stress-strain curve of the tensile process is shown in Fig. 3. Seeing from the following simulations, the strain of the blood vessels cannot exceed 5%, so the ratio of stress and strain when the strain is in 0-5% was regarded as the elastic modulus of the dogbones.

Sample	Thickness/mm	Width/mm
Design	2.0	3.0
Without cells	1.968	2.986
With cells	1.905	2.896

Table I The dimentions of the samples



Fig. 2 DMA machine

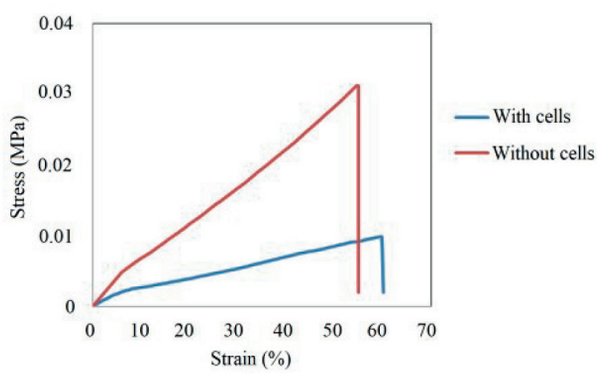


Fig. 3 Stress–strain curve

Fig. 3 shows the stress–strain curves of the dogbones with and without cells based on the tensile tests by DMA machine. The elastic moduli of the dogbone with and without cells were approximately 41 and 80 kPa, respectively. The material without cells was broken when the stress reached 31.80 kPa with the elongation of 54.90%, and the material with cells was damaged when the stress reached 9.84 kPa with the elongation of 60.15%.

Table II summarizes the mechanical properties of the printed samples. Cell addition increased the internal void of hydrogel and reduced the elastic modulus, tensile strength, and stiffness of the materials.

Samples	Strength/kPa	Elongation/%	E/kPa
Without cells	31.80	54.90	80
With cells	9.84	60.15	41

Table II Mechanical properties of the samples

3.4. CELL VIABILITY STUDIES

The cell viability (NIH 3T3 fibroblasts) of the printed hydrogel was studied. Living and dead cells were labeled by CellTracker Green Calcein AM dye and EthD-III, respectively.

The fluorescent viability was obtained and is shown in Fig. 4, in which the green dots represent living cells, and the red dots represent dead cells. The viability rate of NIH 3T3 fibrobalst cells was above 85%, indicating that the printed formulation has low toxicity and minimal influence on cell viability[32].

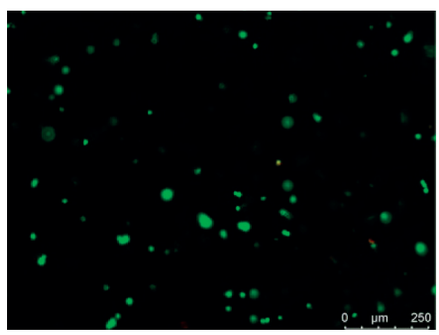


Fig. 4 Fluorescent viability

4. SIMULATION

4.1. MODELS OF FLUID–SOLID INTERACTION

The Workbench module of ANSYS can be used in the simulation of fluid–solid interaction. The simulation analysis covers two parts, one is the hydrodynamic analysis involved with the velocity field of the blood in the vessel, and the other is the structural analysis of the vessel. For the good convergence of the model, a constant dynamic viscosity was assumed for the blood. The one-way fluid–solid interaction method contributed to increasing the convergence of the solution.

The solid model for blood vessel in Workbench used the elastic and isotropic model, and the geometric dimensions of the model are shown in Fig. 5. In this way, two models were built. Their elastic moduli are 80 and 41 kPa (Table II). The Poisson's ratio is 0.45, and the wall density is 1,050 kg/m^3.

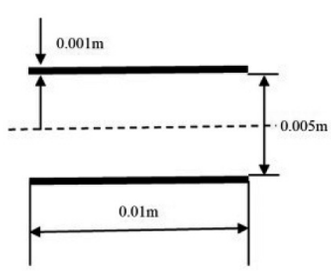


Fig. 5 Tube dimension

The fluid model is based on blood flow in normal human physiological state. The Reynolds number can determine the blood flow pattern. The calculation formula for the Reynolds number is expressed as follows:

$$R_e = \frac{v \cdot D \cdot \rho}{\mu} \quad (1)$$

where v, ρ, and μ represent the velocity, density, and dynamic viscosity of blood, respectively, and D is the vessel diameter. The

outer diameter of the vessel was set to 7 mm, and the thickness was set to 1 mm. The density is 1,060 kg/m^3, the average blood velocity is 0.14 m/s, and the dynamic viscosity is 0.0035 Pa•s. Therefore, the Reynolds value is approximately 300, which is less than 2,300 and thus indicates that the blood flow is laminar.

For the fluid model, the following Navier Stokes equations for incompressible, laminar, and Newtonian viscous fluid were applied:

$$\begin{cases} \rho \cdot U \cdot (\nabla U) = \nabla(-\rho + \mu \cdot (\nabla U + (\nabla U)^T)) \\ \nabla U = 0 \end{cases} \quad (2)$$

where U represents blood flow velocity, and ρ represents the fluid density. The model of fluid–solid interaction in Workbench is shown in Fig. 6.

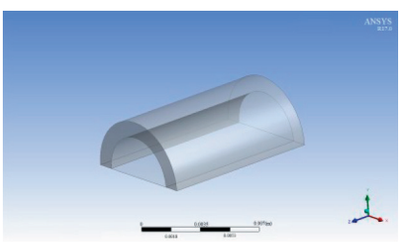


Fig. 6 Tube model

4.2. BOUNDARY CONDITIONS

The velocities of the inlet at four points of time from literature[33] were used and are shown in Fig. 7. The time points are T1 (0.04 s), T2 (0.08 s), T3 (0.20 s), and T4 (0.28 s), representing the accelerated ejection period, ejection peak, reduced ejection period, and early diastolic period, respectively. The boundary condition of the inlet is the velocity, the relative pressure of the outlet is zero, and the flow of blood in the atria is in non-slip condition.

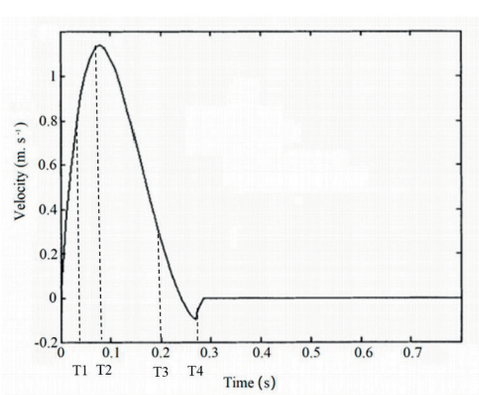
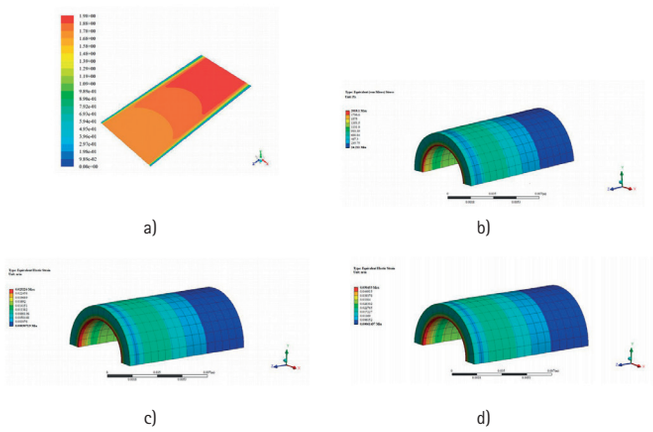


Fig. 7 Velocity of inlet (in a cardiac cycle)

4.3. SIMULATION RESULTS AND DISCUSSION

Under different inlet velocities, the stress and strain of solid wall and fluid velocity distributions were obtained by finite element calculation of the fluid–solid interaction model. Fluid–solid interaction models with cells and without cells were built in Workbench and are shown in Fig. 6. The same size, meshing, and constraint were set for the two models. Hence, no differences on the calculated fluid velocity distribution and wall stress were observed between such models under the same load. The flow velocity at T2 on the symmetric surface of the fluid models is shown in Fig. 8(a), indicating that the maximum velocity occurred at the outlet. Fig. 8(b) shows the stress distribution of the wall. The strain of the two models varies depending on the difference of elastic modulus. The strain distribution at T2 of the wall at elastic moduli of 80 kPa and 41 kPa is respectively shown in Fig. 8(c) and Fig. 8(d).



(a) Velocity distribution on the symmetric fluid surface
(b) Von Misses stresses of wall
(c) Equivalent elastic strain of without-cell model
(d) Equivalent elastic strain of cell model

Fig. 8 Simulation result of the models at T2

Model	E/kPa	Maximum velocity/m/s	Maximum stress/kPa	Maximum strain
Without cells	80	1.98	2.018	0.025226
With cells	41	1.98	2.018	0.049222

Table III Comparison of the simulation results for the two models

As shown in Fig. 8(a), the maximum flow velocity was found in the center of the atria, and the flow velocity decreased toward the wall. At T2, the flow velocity of the inlet reached the maximum value of 1.98 m/s in an entire cardiac cycle.

In a cardiac cycle, the pressure to the wall occurs when the blood flows through the blood vessel, and the wall stress varies depending on the flow velocities of the inlet. At T1, the heart was in accelerated ejection period, the blood flow was accelerated, and the wall stress increased. At T2, the heart was in peak systolic period, and maximum blood flow and wall stress were observed, shown in Fig. 8(b). At T3, the heart was in reduced ejection period, the blood flow was drastically deccelerated, and the wall stress decreased. At T4, the heart was in diastole period, the minimum blood flow was occured, and the wall stress greatly decreased. At T2, the wall stress reached the maximum value of 2,018 Pa.

As shown in Fig. 8(c) and Fig. 8(d), the two models showed maximum strain values of 0.025226 and 0.049222 at T2. Furthermore, the deformation of the model with cells was larger than that of the model without cells. The comparison of the results for the two models is shown in Table III.

5. CONCLUSION

The fluid inlet velocities under four different periods in a cardiac cycle was selected to measure the mechanical properties of 3D printing materials, discover the relationship between the blood flow velocity and 3D-printed blood vessels, and analyze the

fluid flow velocity distribution and the stress and strain of the blood vessels. The following conclusions were drawn:

(1) The hydrogel formula has low toxicity. After cell addition, the mechanical properties of the material were affected, showing reduced strength and stiffness. Under normal blood supply condition, the blood vessels of both materials can meet the strength requirements.

(2) When the vessel inlet velocity increased, the fluid velocity in vessels also increased, and the radial velocity from the center to the wall decreased.

(3) The vessel inlet velocity is proportional to the stress and strain of the solid tube. The vessels with cells were greatly deformed compared with those without cells under the same velocity.

The mechanical properties of 3D-printed vascular materials were studied by combining laboratory experiments with numerical simulation. The relationship between the inlet velocity of fluid and the stress and deformation of 3D-printed blood vessels was proposed to provide reference for the clinical research of 3D bio-printed vessels. Autogenous vessels have three layers, and each layer has different cellular components, stiffness, and functions.

Owing to the limitation of materials and printing accuracy, 3D-printed blood vessels and autologous vessels still differ in terms of mechanical properties and biocompatibility. In the future, 3D printing models will be modified to achieve similarity to autologous vessels, and the controllability and accuracy of printing process will be improved to greatly promote the clinical application of 3D-printed blood vessels.

REFERENCES

[1] Esmaeili S, Shahali M, Kordjamshidi A, et al. "An artificial blood vessel fabricated by 3D printing for pharmaceutical application". Nanomedicine Journal, Summer 2019, Vol. 6-3, p.183-194. DOI: https://dx.doi.org/10.22038/nmj.2019.13183

[2] Gu JY, Gui YS, Chen LR, et al. "CVDHD: a cardiovascular disease herbal database for drug discovery and network pharmacology". Journal of Cheminformatics, December 2013, Vol. 5-1, p.51. DOI: https://dx.doi.org/10.1186/1758-2946-5-51

[3] Shin'oka T, Matsumura G, Hibino N, et al. "Midterm clinical result of tissue-engineered vascular autografts seeded with autologous bone marrow cells". The Journal of Cardiovascular Surgery, June 2005, Vol. 129-6, p.1330-1338. DOI: https://dx.doi.org/10.1016/j.jtcvs.2004.12.047

[4] Williams SK, Morris ME, Kosnik PE, et al. "Point-of-Care Adipose-Derived Stromal Vascular Fraction Cell Isolation and Expanded Polytetrafluoroethylene Graft Sodding". Tissue Engineering Part C: Methods, August 2017, Vol. 23-8, p.497-504. DOI: https://dx.doi.org/10.1089/ten.tec.2017.0105

[5] Lawson JH, Glickman MH, Ilzecki M, et al. "Bioengineered human acellular vessels for dialysis access in patients with end-stage renal disease: Two phase 2 single-arm trials". The Lancet, May 2016, Vol. 387-10032, p.2026-2034. DOI: https://dx.doi.org/10.1016/S0140-6736(16)00557-2

[6] McAllister TN, Maruszewski M, Garrido SA, et al. "Effectiveness of haemodialysis access with an autologous tissue-engineered vascular graft: A multicentre cohort study". The Lancet , 25 April–1 May 2009, Vol. 373-9673, p.1440–1446. DOI: https://dx.doi.org/10.1016/S0140-6736(16)00557-2

[7] Wenger R and Giraud MN. "3D Printing Applied to Tissue Engineered Blood Grafts". Applied Sciences, November 2018, Vol. 8-12, p.2631. DOI: https://dx.doi.org/10.3390/app8122631

[8] Millik SC, Dostie AM, Karis DG, et al. "3D printed coaxial nozzles for the extrusion of hydrogel tubes toward modeling vascular endothelium". Biofabrication, July 2019, Vol. 11-4, 045009. DOI: https://dx.doi.org/10.1088/1758-5090/ab2b4d

[9] Duan B, Hockaday LA, Kang KH, et al. "3D Bioprinting of Heterogeneous Aortic Valve Conduits with Alginate/Gelatin Hydrogels". Journal of Biomedical Materials Research Part A, 2013, Vol. 101-5, p.1255-1264. DOI: https://dx.doi.org/10.1002/jbm.a.34420

[10] Munaz A, Vadivelu RK, St. John J, et al. "Three-dimensional printing of biological matters". Journal of Science: Advanced Materials and Devices, March 2016, Vol. 1-1, p.1-17. DOI: https://dx.doi.org/10.1016/j.jsamd.2016.04.001

[11] Wüst S, Godla ME, Müller R, et al. "Tunable hydrogel composite with two-step processing in combination with innovative upgrade for cell-based three-dimensional bioprinting". Acta Biomaterialia, February 2014, Vol. 10-2, p.630-640. DOI: https://dx.doi.org/10.1016/j.actbio.2013.10.016

[12] Soman P, Chung PH, Zhang AP, et al. "Digital microfabrication of user-defined 3D microstructures in cell-laden hydrogel". Biotechnology Bioengineering, November 2013, Vol. 110-11, p.3038-3047. DOI: https://dx.doi.org/10.1002/bit.24957

[13] Yu Y, Zhang YH and Ozbolat IT. "A hybrid bioprinting approach for scale-up tissue fabrication". Journal of Manufacturing Science and Engineering, December 2014, Vol.136-6, 061013. DOI: https://dx.doi.org/10.1115/1.4028511

[14] Mao W, Lian Q, Li D, et al. "3D printing process for hydro gel with the three-dimensional micro tubes to mimic vascular network". Journal of Mechanical Engineering, September 2017, Vol. 53-9, p.180-186. DOI: https://dx.doi.org/10.3901/JME.2017.09.180

[15] Freeman S, Ramos R, Chando PA, et al. "A bioink blend for rotary 3D bioprinting tissue engineered small-diameter vascular constructs". Acta Biomaterialia, September 2019, Vol. 95-SI, p.152–164. DOI: https://dx.doi.org/10.1016/j.actbio.2019.06.052

[16] Wu W, DeConinck A and Lewis JA. "Omnidirectional printing of 3D microvascular networks". Advanced Materials, June 2011, Vol. 23-24, p.H178-H183. DOI: https://dx.doi.org/10.1002/adma.201004625

[17] Liu HB, Zhou HX, Lan HM, et al. "3D Printing of Artificial Blood Vessel: Study on Multi-Parameter Optimization Design for Vascular Molding Effect in Alginate and Gelatin". Micromachines, July 2017, Vol. 8-8, p.237. DOI: https://dx.doi.org/10.3390/mi8080237

[18] Hoch E, Tovara GEM and Borchers K. "Bioprinting of artificial blood vessels: Current approaches towards a demanding goal". European Journal of Cardio-Thoracic Surgery, November 2014, Vol. 46-5, p.767-778. DOI: https://dx.doi.org/10.1093/ejcts/ezu242

[19] Gaebel R, Ma N, Liu J, et al. "Patterning human stem cells and endothelial cells with laser printing for cardiac regeneration". Biomaterials, December 2011, Vol. 32-35, p.9218-9230. DOI: https://dx.doi.org/10.1016/j.biomaterials.2011.08.071

[20] Kucukgul C, Ozler SB, Inci I, et al. "3D bioprinting of biomimetic aortic vascular constructs with self-supporting cells". Biotechnology Bioengineering, April 2015, Vol. 112-4, p.811-821. DOI: https://dx.doi.org/10.1002/bit.25493

[21] Yu JT, Gong YP, Cui CC, et al. "The FEA model for the prediction of circular tube 3D printing path". Chinese Journal of Applied Mechanics, March 2018, Vol. 35-2, p.440-444. DOI: https://dx.doi.org/10.11776/cjam.35.02.D026

[22] Xu CX, Zhang M, Huang Y, et al. "Study of droplet formation process during drop-on-demand inkjetting of living cell-laden bioink". Langmuir: The ACS Journal of Surfaces & Colloids, July 2014, Vol. 30-30, p.9130-9138. DOI: https://dx.doi.org/10.1021/la501430x

[23] Zhang YH, Yu Y, Akkouch A, et al. "In vitro study of directly bioprinted perfusable". Biomaterials Science, January 2015, Vol. 3-1, p.134-143. DOI: https://dx.doi.org/10.1039/C4BM00234B

[24] Gao G, Lee JH, Jang J, et al. "Tissue Engineered Bio-Blood-Vessels Constructed Using a Tissue-Specific Bioink and 3D Coaxial Cell Printing Technique: A Novel Therapy for Ischemic Disease". Advanced Functional Materials, September 2017, Vol. 27-33, 1700798. DOI: https://dx.doi.org/10.1002/adfm.201700798

[25] Jia WT, SelcanGungor-Ozkerim P, Zhang SY, et al. "Direct 3D bioprinting of perfusable vascular constructs using a blend bioink". Biomaterials, November 2016, Vol. 106-1, p.58. DOI: https://dx.doi.org/10.1016/j.biomaterials.2016.07.038

[26] Miller JS, Stevens KR, Yang MT, et al. "Rapid casting of patterned vascular networks for perfusable engineered three-dimensional tissues". Nature Materials, September 2012, Vol. 11-9, p.768-774. DOI: https://dx.doi.org/10.1038/nmat3357

[27] Lee V, Singh G, Trasatti JP, et al. "Design and fabrication of human skin by three-dimensional bioprinting". Tissue Engineering Part C: Methods, June 2014, Vol. 20-6, p.473-484. DOI: https://dx.doi.org/10.1089/ten.tec.2013.0335

[28] Ho D, Squelch A and Sun ZH. "Modelling of aortic aneurysm and aortic dissection through 3D printing". Journal of Medical Radiation Sciences, March 2017, Vol. 64-1, p.10-17. DOI: https://dx.doi.org/10.1002/jmrs.212

[29] Moore RR, Wallen WJ, Riggs KW, et al. "Three-dimensional printing in surgical planning: A case of aortopulmonary window with interrupted aortic arch". Annals of Pediatric Cardiology, May 2018, Vol. 11-2, p.201-203. DOI: https://dx.doi.org/10.4103/apc.APC_127_17

[30] Gosnell J, Pietila T, Samuel BP, et al. "Integration of Computed Tomography and Three-Dimensional Echocardiography for Hybrid Three-Dimensional Printing in Congenital Heart Disease". Journal of Digital Imaging, April 2016, Vol. 29-6, p.665-669. DOI: https://dx.doi.org/10.1007/s10278-016-9879-8

[31] Wang GL, Sun YN, Yao JY, et al. "Influence of small diameter artificial vessel wall structure on liquid flow field". Transducer and Microsystem Technologies, October 2019, Vol. 38-10, p.4-7. DOI: https://dx.doi.org/10.13873/J.1000-9787(2019)10-0004-04

[32] MAO HL, GU ZW. "Polymers in 3D Bioprinting: Progress and Challenges". Materials China, December 2018, Vol. 37-12, p.949-993. DOI: https://dx.doi.org/10. 7502/j.issn.1674-3962. 2018.12.02

[33] Demirel S, Chen D, Mei Y, et al. "Comparison of morphological and rheological conditions between conventional and eversion carotid endarterectomy using computational fluid dynamics – a pilot study". Vascular, October 2015, Vol. 23-5, p.474-482. DOI: https://dx.doi.org/10.1177/1708538114552836

ACKNOWLEDGEMENTS

This study was supported by the project of Shandong Province Natural Science Foundation, China (No. ZR2017LA005) and that of Shandong Province Higher Educational Science and Technology Program (No. J16LJ11).
We also thank Dr. Changxue Xu of Texas Tech University for his help and advice.